AIMS Materials Science, 3(2): 508-524.
DOI: 10.3934/matersci.2016.2.508
Received: 22 February 2016
Accepted: 11 April 2016
Published: 18 April 2016

http://www.aimspress.com/journal/Materials

Research article

Photoluminescence engineering in polycrystalline ZnO and ZnO-based compounds

Iryna Markevich, Tetyana Stara, Larysa Khomenkova, Volodymyr Kushnirenko, and Lyudmyla Borkovska *

V. Lashkaryov Institute of Semiconductor Physics, 45 Pr. Nauky, 03028 Kyiv, Ukraine

* **Correspondence:** Email: l_borkovska@ukr.net; Tel: +38-044-5256340; Fax: +38-044-5258342.

Abstract: The results of the investigations of photoluminescence (PL) in ZnO and ZnO-based composite materials are presented. The PL and PL excitation (PLE) spectra of undoped and doped with I group elements or rear earth ions ZnO polycrystalline films, ZnO, $Zn_{1-x}Mg_xO$ and ZnMgO–TiO_2 ceramics were studied. The structural properties of the samples were investigated with X-ray diffraction. Polycrystalline films were prepared by a screen-printing method and annealed at T_S = 500–1000 °C. The films annealed at T_S < 800 °C exhibited intense UV emission, whereas defect-related one appeared at 800 °C and enhanced with increasing T_S. Improvement of the PL and structural characteristics of ZnO films due to Li-doping were achieved. The PL bands caused by Sm and Ho ions were observed under ZnO band-to-band excitation. In the PL spectra of ZnO and $Zn_{1-x}Mg_xO$ ceramics, two types of PL bands were separated: i) the bands, whose spectral positions were not influenced by the Mg content (green Cu-related as well as self-activated orange and red ones); ii) the bands, spectral positions of which exhibited some blueshift with increasing Mg content (orange Li- and Ag-related and self-activated green ones). In the PL spectra of ZnMgO–TiO_2 composites, an intense red emission was found to appear in addition to the broad blue-orange band inherent in ZnMgO alloy. The red emission was ascribed to Mg_2TiO_4 inclusions in ZnMgO matrix.

Keywords: ZnO**;** ZnMgO; ZnMgO–TiO_2; ceramics; films; screen-printing; defects; doping; photoluminescence; photoluminescence excitation; rear earth

1. Introduction

Unique electrical and optical properties of ZnO side by side with its high thermal and optical stability, high radiation hardness, low cost and the absence of toxicity make this compound an excellent candidate for electronics device applications [1,2]. In particular, zinc oxide attracts much attention as a promising material for emitters of both UV and visible light [1,3]. Visible emission of ZnO is known to consist of a number of bands related to different lattice defects. The large LO-phonon energy (72 meV) and strong phonon-electron coupling in ZnO cause the broadening of emission bands, which leads to their essential overlapping. As a result, defect-related emission in ZnO exhibits itself as a broad unstructured band spreading from blue to red spectral regions. This peculiarity makes ZnO a prospective phosphor for white-light emitters with a high color rendering index [3]. At the same time, such an overlapping impedes the separation of broad band components and the determination of their peak positions, which can account for the discrepancies in reported data. The origin of emission centers and carrier transitions responsible for emission in ZnO are also the subject of discussion thus far. So, further investigations of ZnO defect-related emission and the influence of different treatments on its spectrum shape and intensity are required. Besides, the possibility of UV emission enhancement in polycrystalline ZnO should be found. In present paper, our recent results on the investigation of light emitting properties of polycrystalline ZnO and ZnO-based materials [4–9] are given. It is shown that tuning of sintering conditions and composition of starting charge enables monitoring luminescent spectrum from the UV to the red.

2. Materials and Method

Sintering of ceramics is one of the most attractive methods of ZnO material fabrication due to its simplicity, low cost and the possibility to modify material characteristics in wide range by introduction of different additives in the starting charge. In turn, screen-printing is a very simple and viable technique to produce thick films of various materials. It ensures maximum material utility and offers a suitable method for preparing films on large area substrates.

Investigated samples were undoped and doped with I group elements ZnO, ZnMgO and ZnMgO–TiO_2 ceramics as well as undoped and doped with Li^+, Ho^{3+} and Sm^{3+} ions polycrystalline ZnO layers prepared by a screen-printing method [10].

Ceramic samples were formed of the mixture of ZnO, MgO and TiO_2 powders (all of 99.99% purity) with distilled water or $LiNO_3$, $AgNO_3$ and $CuSO_4$ aqueous solutions. In $Zn_{1-x}Mg_xO$ samples, x was varied from 0 to 0.20. In doped samples, impurity concentration was about 10^{18} cm^{-3}. In $Zn_{1-x}Mg_xO$–TiO_2 composites, x = 0.30–0.40 and TiO_2 contents were 10 and 12.5 wt%. To investigate the influence of adding TiO_2 on ZnMgO alloy emission, $ZnTiO_3$, Zn_2TiO_4, $MgTiO_3$ and Mg_2TiO_4 titanates were also prepared. For this purpose, ZnO, MgO and TiO_2 oxides were mixed according to stoichiometry ratio. The samples were dried at room temperature, sintered in air for 3 h at T_S = 1100 °C and cooled with the furnace. A number of samples were sintered in the N_2 flow or Zn vapor. In the last case, the samples were located in a closed alumina crucible with metallic Zn scraps and annealed in N_2 flow. In all cases, dense ceramics with average sizes of 10 × 3 × 2 mm^3 were obtained. Sintered ceramic samples were cut transversally and the PL was measured from the cleft surface.

The films were produced by screen-printing of a ZnO-based paste on the non-polished (1012) Al_2O_3 substrates of 1 × 1 cm^2 areas, dried at room temperature under atmospheric conditions and

sintered in air at T_S = 800–1000 °C for 30 min and 60 min. The paste was prepared of Sigma–Aldrich ZnO powder (99.99% purity) mixed with distilled water or $LiNO_3$ aqueous solution. To produce the films doped with rare-earth (RE) ions, the ZnO powder was mixed with RE_2O_3:H_2O:HCl solutions of different composition. The Ho_2O_3 (99.95%) and Sm_2O_3 (99.95%) were used as the RE sources. The concentration of Li dopant in the films varied from 1.4×10^{19} to 1.4×10^{21} cm^{-3}, while concentration of rare-earth ions was in the range of (2–4) $\times 10^{20}$ cm^{-3}. The thickness of sintered films was about 40 μm.

The photoluminescence (PL) and PL excitation (PLE) spectra of the films and ceramic samples were recorded using a SDL-2 spectrometer (LOMO, St. Petersburg) equipped with a photomultiplier tube sensitive in 200–900 nm spectral range. The PL was excited by a pulsed N_2-laser (337.1 nm; the pulse duration was 7 ns; the repetition frequency was 100 Hz), a 407-nm continuous-wave diode laser (~40 mW) and by a Xe lamp (150 W). The latter was also used for PLE measurements. X-ray diffraction (XRD) study was realized using X-ray powder diffractometer ARL X'TRA with the Cu $K\alpha_1$ and Cu $K\alpha_2$ radiation. The PL and PLE investigations were performed at 77K and 293K.

2. Results and Discussion

2.1. Ceramic samples

2.1.1. Zinc oxide

The most of investigators believe that defect-related emission in intentionally undoped ZnO consists of green and orange ones [1,2]. The green emission, in its turn, includes two bands, one of which is due to stoichiometric Zn excess and the other is related to residual copper impurity [1,2]. Self-activated orange emission is observed, as a rule, in the samples annealed in air or oxygen ambient and is associated with stoichiometric oxygen excess [11–14]. Peak positions of emission bands, however, have not been determined reliably. In particular, quite different values from 570 to 640 nm can be met in the literature for peak position of self-activated orange band [11–14]. One of the reasons of such a spread can be the fact that the separation of overlapping bands and determination of their peak positions are often made using Gaussian fitting procedure. At the same time, Gaussian deconvolution of a broad unstructured band will be rather ambiguous if the number and pick positions of components are unknown. More reliable results can be obtained when the positions of some bands are preliminarily established. In the present work, self-activated orange band was separated by Gaussian deconvolution of PL spectrum using peak positions of the other components obtained experimentally.

To determine peak positions of green self-activated and Cu-related bands, PL spectra of ZnO ceramics sintered in Zn vapor as well as doped with Cu were measured. It was found that the samples sintered in Zn vapor demonstrated extremely intense green emission peaked at 515 nm (Fig.1, curve 1), whereas green band with peak position at 540 nm dominated in PL spectra of Cu-doped samples (Fig.1, curve 2). It should be noted that emission in red spectral region was also observed in undoped ZnO. This emission looked usually as a shoulder on the longer-wavelength side of the orange one, but sometimes exhibited itself as a distinct band at about 700 nm [12,15]. In some of our undoped ZnO samples, a distinct red PL band peaked at 720 nm was observed in addition to green and orange emissions (Fig.1, curve 3). PL spectrum of undoped ZnO sample sintered in air and its Gaussian deconvolution are shown in Fig.1 (curve 4). The deconvolution was made taking into account obtained

peak positions for two green bands (515 and 540 nm) as well as for self-activated red one (720 nm). As a result, the orange band peaked at 610 nm was separated.

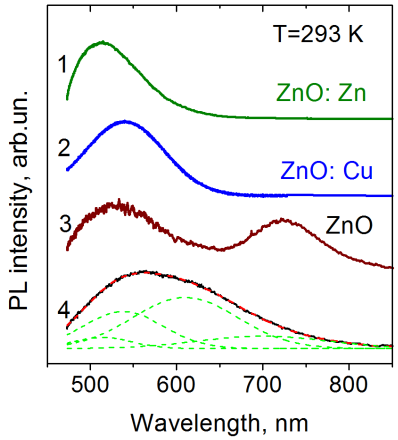

Figure 1. PL spectra of ZnO ceramics sintered in Zn vapor (1), doped with Cu (2), undoped one that demonstrated a distinct red PL band (3) and Gaussian deconvolution of typical PL spectrum for undoped ZnO samples sintered in air (4); T = 293 K, λ_{EXC} = 365 nm.

It should be noted that self-activated orange emission in ZnO is usually ascribed to oxygen interstitials [1,11–14]. At the same time, essential enhancement of orange emission side by side with the quenching of green one was observed in high-purity ZnO powder after annealing in vacuum, a layer of metallic zinc being formed on the cold end of silica tube in which the annealing was performed [16]. Based on these facts, it was concluded that emission centers responsible for orange emission are related to zinc vacancies formed due to zinc evaporation [16].

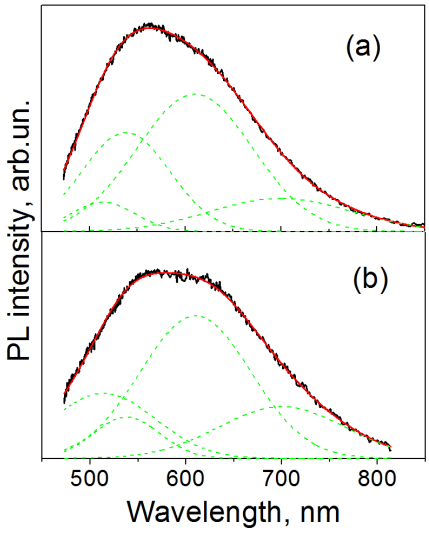

Figure 2. Normalized PL spectra and their Gaussian deconvolution for undoped ZnO ceramics sintered in N_2 flow. The spectra are recorded from the bulk (a) and the surface (b) of the sample; T = 293 K, λ_{EXC} = 365 nm.

This conclusion is confirmed by our experiments. It was found that sintering of undoped ZnO samples in N_2 flow resulted in the increase of contribution of orange emission to PL spectrum, this effect being more pronounced in the sample surface with respect to its bulk (Fig. 2). In fact, one can expect that higher density of zinc vacancies should be formed due to zinc evaporation i) on the surface of the sample with respect to its bulk; ii) under sintering in N_2 flow with respect to that in immobile air due to removal of evaporated Zn from annealing zone by gas stream.

2.1.2. ZnMgO alloys

In recent years, ZnMgO solid solutions attract much attention as promising materials for UV-light emitters. On the other hand, alloying with MgO results in the enhancement of ZnO defect-related emission and, so, these alloys can be considered as potential candidates for visible-light phosphors. At the same time, reported data on the visible emission in ZnMgO compounds are rather scarce and controversial. To investigate the influence of alloying MgO with ZnO on the intensity and spectrum of defect-related emission in ZnMgO solid solutions, undoped and doped with Zn, Cu, Li and Ag ceramics with different Mg content were sintered and their luminescent characteristics were measured. Because of crystal structure dissimilarity between hexagonal ZnO and cubic MgO, these oxides do not show a complete solubility over the entire composition range. With increasing Mg content, at first ZnO-based wurtzite phase is formed, then the separation of the phases with wurtzite and rock-salt structures takes place and, at last, MgO- based rock-salt alloy becomes predominant [17]. XRD patterns of prepared ceramics were measured and analyzed earlier in [18]. It was shown that both hexagonal and cubic ZnMgO phases were formed under sintering, and MgO solubility limit in hexagonal phase was found to be 20 at% [18]. Since only hexagonal phase exhibited noticeable visible emission, $Zn_{1-x}Mg_xO$ samples with x = 0–0.20 were prepared for the PL and PLE measurements.

PL spectra of undoped $Zn_{1-x}Mg_xO$ ceramics look as broad unstructured bands which are similar to those in ZnO. The PLE spectra of undoped $Zn_{1-x}Mg_xO$ samples with different x are plotted in Fig.3. The shift of PLE peak, whose position coincides with that of free exciton [18], toward short-wavelength side with increasing x is the evidence of bandgap broadening due to formation of hexagonal ZnMgO solution, which was proved by X-ray diffraction study [18]. It was found that PLE spectra are identical for all PL bands observed in both undoped and doped samples with the same x.

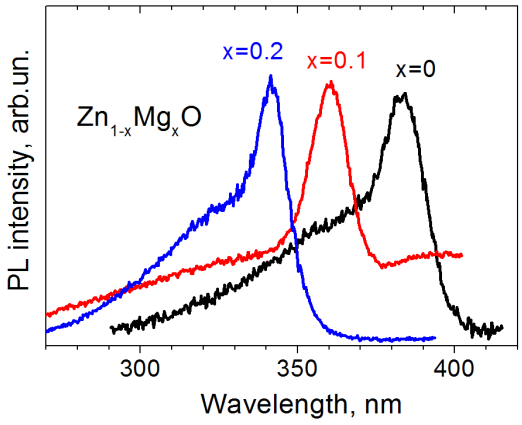

Figure 3. Normalized PLE spectra of $Zn_{1-x}Mg_xO$ ceramics with x = 0, 0.1, 0.2; T = 293 K.

To perform Gaussian deconvolution of the PL spectra of $Mg_xZn_{1-x}O$ samples, the behavior of visible band components depending on x should be clarified. For this purpose, PL spectra of all the doped and undoped $Zn_{1-x}Mg_xO$ samples were measured under excitation by the light $\lambda_{EXC} = 320$ nm corresponding to band-to-band absorption and were analyzed. In ceramics sintered in Zn vapor, the blueshift of self-activated green band from 515 to 485 nm was found to occur with increasing x from 0 to 0.20 (Fig.4a).

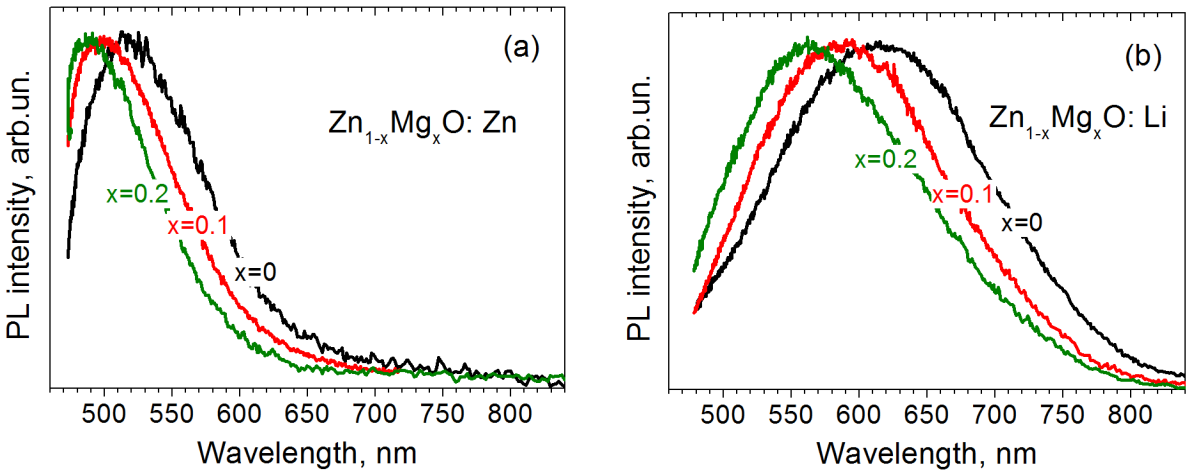

Figure 4. Normalized PL spectra of $Zn_{1-x}Mg_xO$ ceramics with x = 0, x = 0.10 and x = 0.20 sintered in Zn vapor (a) and doped with Li (b); T = 293 K, $\lambda_{EXC} = 320$ nm.

Similar effect was also observed in ceramics doped with Li and Ag. Doping of ZnO with these impurities was shown to cause the appearance of intense orange bands at 600 and 580 nm, respectively [19]. Alloying with MgO resulted in the shift of both Li- and Ag-related bands toward short-wavelength side (Fig.4b, Fig.5a). At the same time, any shift of Cu-related PL band was not observed in $Zn_{1-x}Mg_xO$ samples doped with Cu (Fig.5b). Comparison of the PL spectra for undoped samples with different x demonstrating distinct red band showed that peak position of this band (720 nm) was independent of x (Fig.5, c).

PL spectra of undoped $Zn_{1-x}Mg_xO$ samples with different x are plotted in Fig.5d. Gaussian deconvolution was performed taking in account determined above peak positions of self-activated green and red bands as well as Cu-related one. As a result, orange PL band with the same peak position at 610 nm for each x was separated. One can see that the contribution of this band to the observed PL at first increased and then decreased with increasing x.

Obtained results indicate that two types of emission bands are present in PL spectra of investigated samples: i) the bands whose peak positions are not influenced by Mg content (self-activated orange and red as well as Cu-related ones); ii) the bands whose peak positions show some blue-shift with increasing Mg content (self-activated green as well as Li- and Ag-related ones). Thus, energy levels related to corresponding emission centers demonstrate different reaction to band gap broadening due to alloying ZnO with MgO, which testifies to different interaction of these centers with the host lattice. For the first-type centers, two possibilities should be considered: i) energy level is pinned to the involved allowed band from which carrier recombination on the given center occurred; ii)

the emission is caused by an intra-defect transition, excited and ground states of the center being weakly coupled to the band properties of the host lattice. The latter has been proposed for Cu_{zn} acceptor in ZnO [1,2]. For orange and red self-activated centers, the former possibility seems to be more probable. These bands are usually ascribed to electron transitions from c- band or shallow donors to deep acceptors [1,2,11–15]. The second type centers show the shift of their energy levels with respect to the involved allowed band under bandgap broadening. This shift is about 0.20 eV at x = 0.20 for all second type centers, which is twice as little as that of free exciton (see Fig.3). One can think, therefore, that energy levels of these centers shift equally with respect both to c- and v- bands. It should be noted, however, that electron-hole transitions responsible for specific emission bands in ZnO remain so far highly disputable throughout the literature and further studies in this field are required.

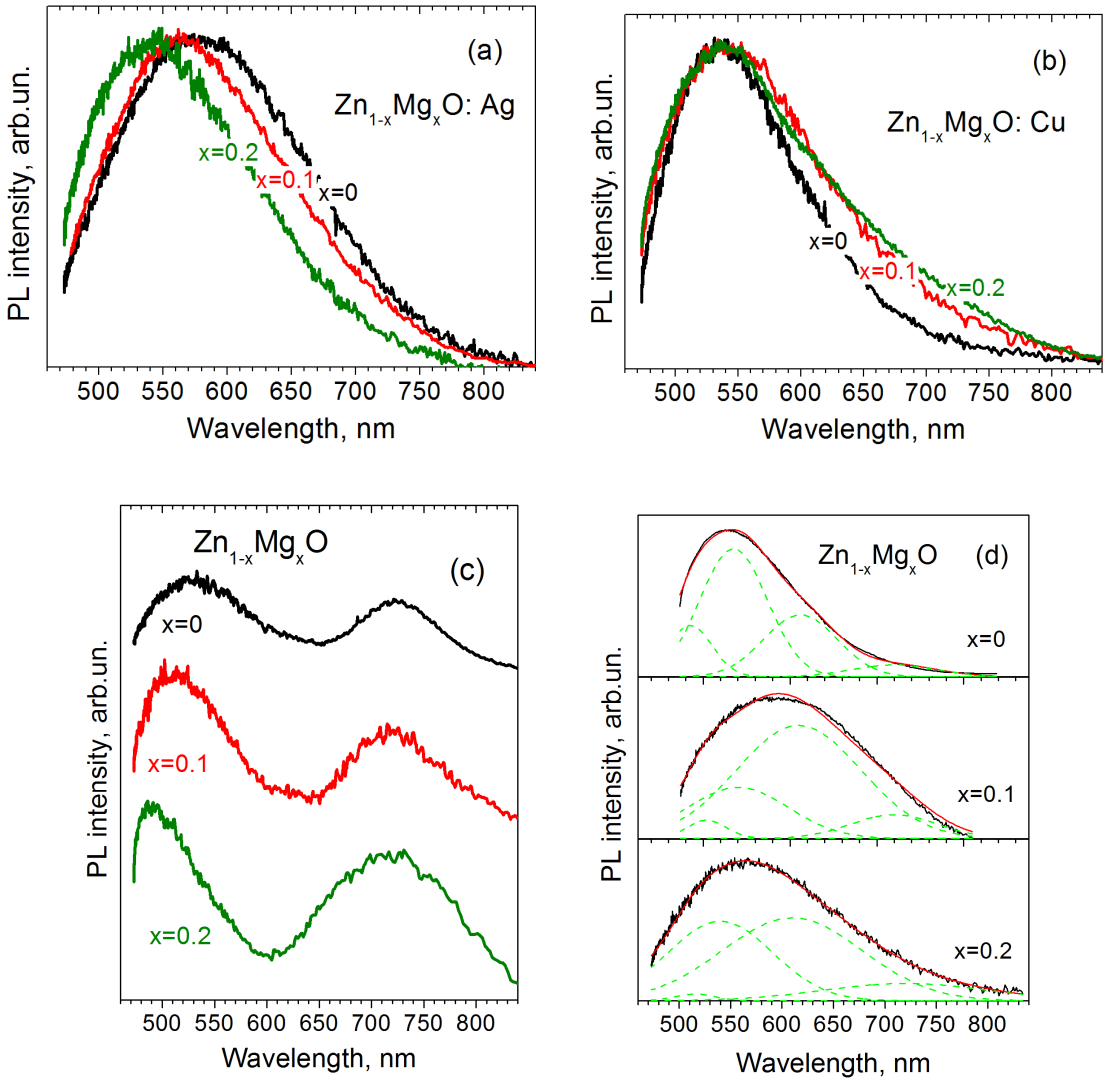

Figure 5. Normalized PL spectra of $Zn_{1-x}Mg_xO$ ceramics with x = 0, x = 0.1 and x = 0.2 doped with Ag (a) and Cu (b); PL spectra of undoped $Zn_{1-x}Mg_xO$ ceramics with x = 0, x = 0.10 and x = 0.20 with distinct red PL band (c) and Gaussian deconvolution of typical PL spectrum for undoped $Zn_{1-x}Mg_xO$ ceramics (d); T = 293 K.

2.1.3. $ZnMgO–TiO_2$ composites

Above results show that bright blue, green, yellow and orange emissions can be obtained in ZnMgO solid solutions by corresponding treatments, while the emission in red spectral range is rather week. At the same time, the enhancement of red emission will enable the fabrication of white-light phosphors based on these alloys.

It is known that zinc and magnesium titanates exhibit strong red emission [20,21]. One can expect that new effective phosphors can be developed using these compounds. In particular, it can be assumed that introduction of titanium oxide in the starting mixture of zinc and magnesium ones will lead to the appearance of red component in emission spectra of prepared ceramics. To verify this assumption, $ZnMgO–TiO_2$ composites as well as $ZnTiO_3$, Zn_2TiO_4, $MgTiO_3$ and Mg_2TiO_4 titanates were sintered and their photoluminescence characteristics were measured. As Fig.6a shows, a distinct red band peaked at 670 nm is present in the PL spectra of $ZnMgO–TiO_2$ composites side by side with a broad blue-orange one inherent in ZnMgO alloys. One can see that relative intensities of these bands can be controlled by the change of both TiO_2 and MgO contents in the starting charge, the peak position of the red band remaining the same.

It was found that the PLE spectra of the broad band components (Fig.6b, curve 1) are identical to those for $Zn_{1-x}Mg_xO$ alloys with $x \geq 0.20$ (see Fig.3), whereas PLE spectrum of the red band is quite different (Fig.6b, curve 2).

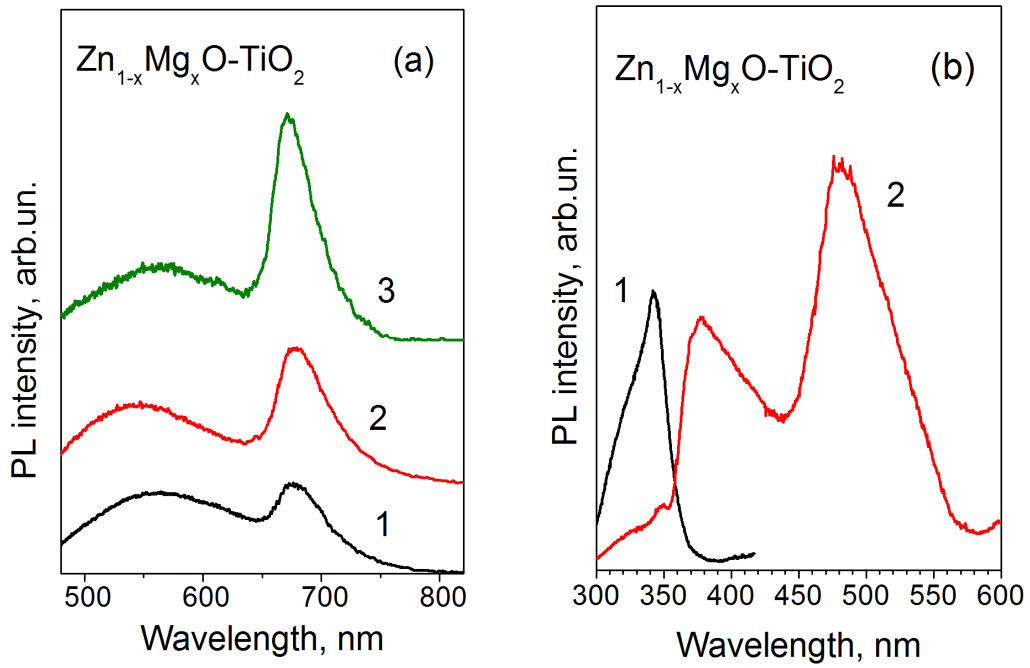

Figure 6. PL spectra of $Zn_{1-x}Mg_xO–TiO_2$ composites normalized with respect to broad band maximum: (1) x = 0.30, 10wt% TiO_2; (2) x = 0.30, 12.5 wt% TiO_2; (3) x = 0.40, 12.5 wt% TiO_2, λ_{EXC} = 365 nm (a), and PLE spectra of broad band components (1) and red band (2) in $ZnMgO–TiO_2$ composites (b); T = 293 K.

Such a difference can indicate that emission centers responsible for the red PL band in composite

samples are not local defects in ZnMgO, but relate to some other substance whose inclusions can form in the host lattice under sintering. Recent structural investigations of ceramics prepared of ZnO and TiO_2 powders showed that $ZnTiO_3$ and Zn_2TiO_4 precipitates were formed in ZnO matrix under sintering and became noticeable at Ti content of 2–3 at% [22,23]. One can suppose, therefore, that the formation of both zinc and magnesium titanates takes place in ZnMgO–TiO_2 composites. To verify this supposition, PL and PLE spectra of prepared zinc and magnesium titanates were measured and compared with those for ZnMgO–TiO_2 composites.

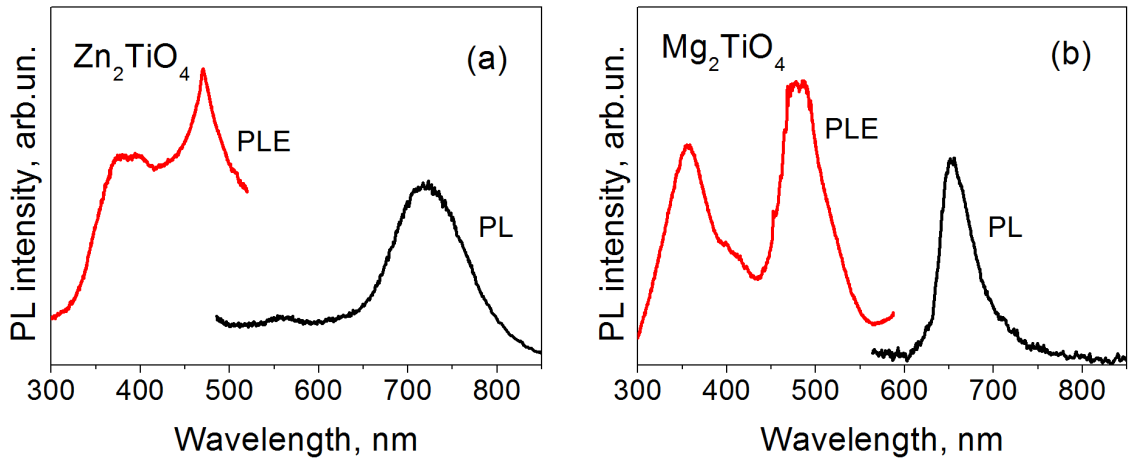

Figure 7. PL and PLE spectra of Zn_2TiO_4 (a) and Mg_2TiO_4 (b) ceramics; λ_{EXC} = 365 nm, T = 293 K.

It was found that $ZnTiO_3$ and $MgTiO_3$ ceramics demonstrated visible emission in wide spectral range, but the intensity of this emission was extremely week. At the same time, red PL bands peaked at 720 and 660 nm were observed in the PL spectra of Zn_2TiO_4 and Mg_2TiO_4 samples, respectively (Fig.7), the PL intensity of Mg_2TiO_4 ceramics being more than ten times stronger than those of Zn_2TiO_4 ceramics. The PLE spectra of these bands (Fig.7) are similar to those for the red emission in ZnMgO–TiO_2 composites (Fig.6b).

The data plotted in Figs.6 and 7 demonstrate that PL and PLE spectra in Zn_2TiO_4 and Mg_2TiO_4 samples exhibit the same characteristic features as those in composites, namely, a distinct red band with a full width at half maximum (FWHM) of about 0.2 eV and an intense long-wavelength PLE maximum in 450–550 nm spectral range which are never observed in ZnMgO alloys. In zinc titanate, however, peak position of the red band (720 nm) is far enough from that in composite material (670 nm) and blue-green PLE maximum is shifted to shorter wavelengths with respect to that in ZnMgO–TiO_2 ceramics. At the same time, the long-wavelength PLE maxima are practically identical for Mg_2TiO_4 and composite materials and only a slight shift is observed between peak positions of red PL bands in Mg_2TiO_4 and ZnMgO–TiO_2 samples (660 and 670 nm, respectively). Based on these facts and taking into account the weakness of red PL band in Zn_2TiO_4 with respect to that in Mg_2TiO_4, one can conclude that Mg_2TiO_4 inclusions formed in composite material under sintering are responsible for the red emission in $Zn_{1-x}Mg_xO$–TiO_2 ceramics. This effect seems to be quite understandable, because, at x > 0.20, "surplus" MgO that does not dissolve in ZnO can take part in the formation of Mg_2TiO_4 phase. In fact, the greater the MgO content, the higher the red emission intensity in composite samples. To elucidate the origin of red emission and the mechanism of its excitation further investigations are

required.

The emission of prepared composites under UV excitation (Fig.6a) is perceived with the naked eye as a bright white light. The tinge of this light can be made warmer or colder by the change of starting charge composition. Obtained results show that ZnMgO–TiO_2 ceramics are promising materials for the development of white-light emitters.

2.2. Polycrystalline films

2.2.1. Effect of Li-doping on the PL of screen-printed ZnO films

An interest to Li-doped ZnO has been motivated mainly by high perspectives for realizing p-type conductivity. In fact, it was theoretically predicted that Li incorporation on the Zn-lattice site (Li_{Zn}) produces a shallow acceptor level [24]. In some reports, it has been demonstrated that upon Li doping at temperatures below 700 °C the shallow acceptors with binding energy of about 300 meV are introduced [25,26]. These shallow acceptors participate in donor-acceptor pair recombination band at 3.05 eV [26]. However, the most of the experimental reports supposed that Li_{Zn} is a deep acceptor with the binding energy of about 800 meV and is responsible for yellow luminescence at 2.0–2.2 eV ascribed to shallow donor to deep acceptor recombination [19,27,28]. Therefore, Li can be used also for producing visible luminescence in the yellow spectral range.

The undoped ZnO films were sintered at 500–1000 °C for 0.5–1 h. It has been found that the films annealed at temperatures lower than 800 °C show intense UV emission and weak defect-related PL band. The PL spectra of the films sintered at 800 °C and higher temperatures showed gradual decrease of the UV luminescence and the increase of defect-related PL.

To study the effect of Li-doping, the ZnO films with different Li content (1.4×10^{19}, 1.4×10^{20} and 1.4×10^{21} cm^{-3}) were sintered in air at 800 °C for 0.5 h. The room-temperature and low-temperature luminescence spectra of Li-doped ZnO films are shown in Fig.8a and Fig.8b, respectively. In the PL spectra, the UV band, I_{UV}, and the wide defect-related band, I_{DEF}, in the green-orange spectral range are observed. The UV band is a superposition of exciton-related bands of ZnO. As the temperature is decreased from 293 to 77 K, the UV band divides into several clearly resolved PL peaks that can be ascribed to a donor-bound exciton band I_D (369 nm) as well as to three phonon replicas of free A-exciton (374, 383 and 392 nm) (Fig.9a).

The relative intensity of the UV and visible defect-related bands are found to depend significantly on Li content. The undoped film shows rather low intensity of the UV band, while the doped ones show strongly enhanced UV emission. At the same time, the highly doped film ([Li] = 1.4×10^{21} cm^{-3}) does not demonstrate any exciton-related PL both at room and low temperatures. Moreover, in the room-temperature PL spectra of the highly-doped film, the defect-related PL is decreased too. The ratios of the intensities of the UV and defect-related PL bands (I_{UV}/I_{DEF}) shown in Fig.9b enables estimating the structural performance of ZnO films. The best PL properties are found for lightly doped films ([Li] = 1.4×10^{19} cm^{-3}) whereas the highly doped film is the worst.

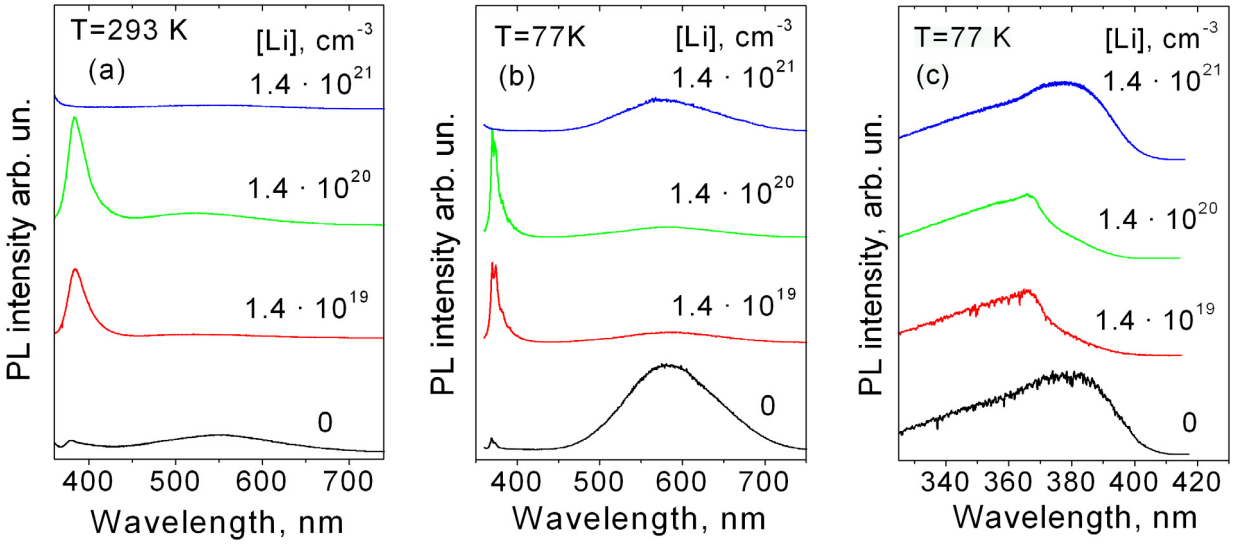

Figure 8. PL (a, b) and PLE (c) spectra of undoped and Li-doped ZnO films with different content of Li (1.4×10^{19}, 1.4×10^{20} and 1.4×10^{21} cm^{-3}) recorded at 293 K (a) and 77 K (b, c). $\lambda_{EXC} = 337.1$ nm. PLE spectra are recorded at 580 nm.

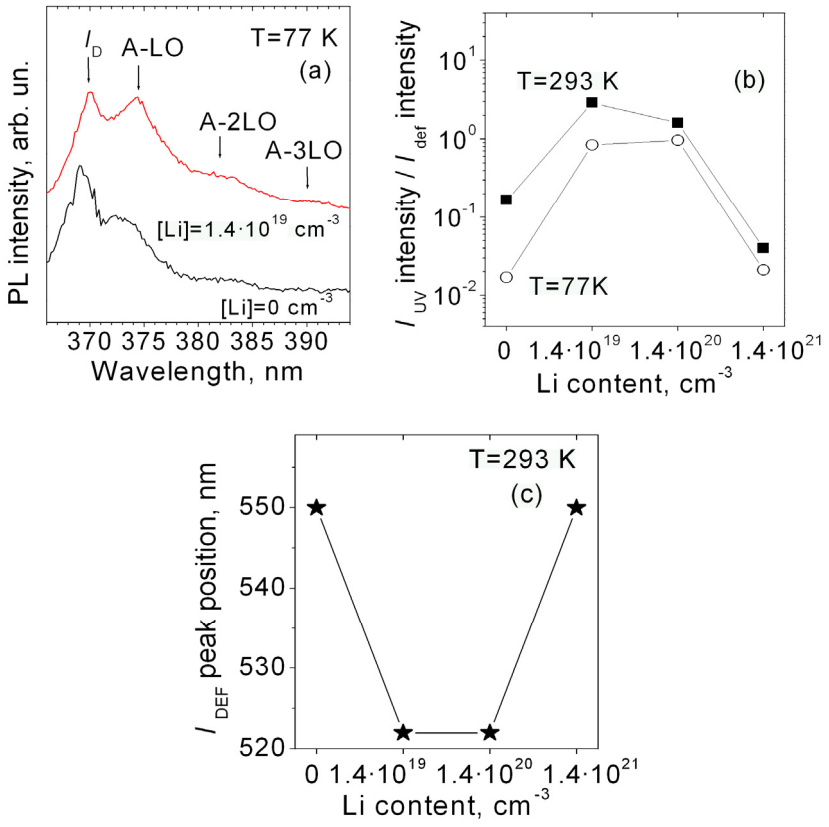

Figure 9. PL spectra of the undoped and Li-doped ZnO films (a); ratio of integrated intensities of excitonic to defect-related bands (b) and spectral position of defect-related band (c) versus Li content; $\lambda_{EXC} = 337.1$ nm.

An improvement of structural perfection of ZnO films upon Li-doping is proved by the excitonic spectra, where the increase in the intensity of the phonon replicas of free A-exciton relative to that of bound exciton emission is found (Fig.9a). In the room-temperature PL spectra, this effect appears in the shifting of the UV band maximum from 378 nm in the films with low UV emission to 384 nm in the films with strongly enhanced UV PL. Spectral position of the I_{DEF} band maximum also changed in the doped films. It varies in the range of 522–550 nm in different samples and shows the shortest wavelength position for the Li-doped films with [Li] = 1.4×10^{19} and 1.4×10^{20} cm^{-3} (Fig. 9c). This indicates that the defect-related PL band is complex and composes of at least two overlapping PL bands (green and orange bands).

The low-temperature PLE spectra recorded in the maximum of the defect-related band are shown in Fig. 8c. In the PLE spectra, the band-to-band ($\lambda_{EXC} < 365$ nm) and free exciton (~369 nm) absorption features as well as some defect-related absorption peak at about 380–385 nm are found. The defect-related peak is observed in the low-temperature PLE spectra of the orange PL band, but is not found for the green emission.

The results of the PL study clearly indicate that Li-doping affects strongly crystal structure of the films. The doping with Li of low concentrations improves it, while the high concentration of Li dopant degrades it. The decrease of the total PL intensity upon high Li concentrations can be due to concentration's quenching of the PL intensity by dopants. In the films with improved crystal structure, the green PL band dominates, while in more defective films (the undoped and highly doped films), the orange emission prevails. At the same time, neither a pronounced increase in the intensity, nor the evident shift of the I_{DEF} peak position are observed in the ZnO:Li films as compared with the undoped films. This hinders an identification of Li-related emission in the doped films. So, in spite of the fact that the orange band is often ascribed to Li_{Zn} acceptor we cannot exclude that in the ZnO:Li films this band originates from the intrinsic defects of ZnO mainly.

The effect of Li-doping on the ZnO crystallization processes is proved by the XRD study. The XRD patterns of undoped and Li-doped ZnO films show the peaks corresponded to polycrystalline wurtzite ZnO without preferable grain orientation (Fig.10a). For doped film with Li content of 1.4×10^{19} cm^{-3}, the diffraction peaks are shifted towards smaller angles and the peaks became narrower as compared with the undoped film, while further increase of Li concentration produces the opposite effect, i.e. the peak shifting to larger angles and FWHM increase. Assuming a homogeneous strain across the films, the crystallite sizes were evaluated from the FWHM for different XRD peaks using the Scherrer's equation. The representative behavior of the grain sizes in dependence on Li content is shown in Fig.10c for a (002) diffraction peak. The introduction of Li in low concentration is found to promote nanocrystal growth, while high Li content hinders this process. The nature of the former effect is not clear now, while the latter can be caused by segregation of insoluble Li atoms at the grain boundaries, which suppress growth of nanocrystals [29]. The increase of the grain sizes upon Li-doping results in lower density of extended defects such as subgrain boundaries. It can be assumed that the increase of grain sizes affects also the formation of vacancy and interstitial defects inside the crystallites as well as stimulates defect diffusion during crystal growth.

Therefore, Li doping in low concentration of 1.4×10^{19} cm^{-3} enables producing the films with enhanced UV emission, reduced density of crystalline defects and larger grain size. This enables decreasing thermal budget for film production. Similar effect of improvement of optical and structural properties of zinc oxide nanowires after indium doping have been reported in [30 and references ibid]. At the same time, introduction of high amount of Li produces an additional structural disordering and

the degradation of the whole PL spectrum. The obtained results indicate that Li-doping is seems to be ineffective in producing an intense yellow luminescence in the films studied.

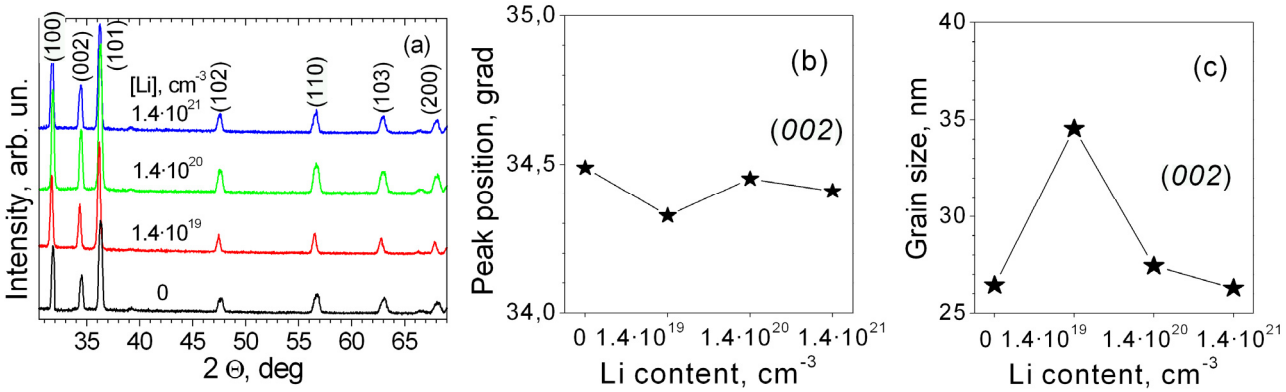

Figure 10. XRD patterns (a), ZnO (002) peak position (b) and grain sizes (c) of undoped and Li-doped ZnO films vs Li concentration.

2.2.2. Effect of RE-doping on the PL of screen-printed ZnO films

Introduction of rare-earth (RE) ions in semiconductor materials is considered as an efficient way to produce emission in specific spectral range. The 4f orbital of RE ions is shielded from the surroundings by the filled $5S_2$ and $5P_6$ orbitals that minimized the influence of the host lattice on the optical transitions within the 4f configuration [31]. Moreover, their 4f states only weakly interact with the host lattice, and therefore the energy differences are nearly constant, leading to almost the same emission spectra in different host lattices [32,33].

To achieve PL bands in the green and red spectral regions the ZnO films were doped with Ho and Sm ions, respectively. The RE ions of two types were introduced in the ZnO both separately (RE doped films) and simultaneously (codoped films) from the corresponding oxides during film sintering. The latter was done in the air at 1000 °C for 1 h. The concentrations of Ho and Sm dopants were about 2×10^{20} cm^{-3} and in the range of $(2–4) \times 10^{20}$ cm^{-3}, respectively.

The low-temperature PL spectra of the undoped and RE doped films under ZnO band-to-band excitation are presented in Fig.11. The PL spectra of the films doped with one type of RE ions (Fig.11a) show the same PL bands as the undoped ZnO with no variations in the PL band position. No fingerprint of the self-emission of Ho^{3+} or Sm^{3+} ions is found. In the PL spectra of the Ho-doped film, the intensity of the UV band exceeds that of the visible PL. This attests that the doping of ZnO with Ho^{3+} ions enables crystalline structure of the films to be improved.

In the PL spectra of the codoped films (Fig.11b), a significant quenching (more than 5 times) of total PL intensity was observed, the UV emission being quenched prominently. On a background of the weak defect-related PL of ZnO host, some additional peaks in the 460–500 nm and 680–730 nm spectral ranges appeared. The latter set of narrow peaks is found on a background of red self-activated PL band at ~720 nm. These peaks can be ascribed to the emission of RE ions themselves. By using the Dieke diagram from [31] the peaks in the range of 460–480 nm can be assigned to the $^5F_1 \rightarrow {}^5I_8$ transitions in Ho^{3+} ions (Fig.12). At the same time, the peaks in 680–730 nm range cannot be attributed to the optical transitions in Sm^{3+} ions that show no emission in this region. The most probable origin of

this emission is the Sm^{2+} ions whose $^5D_0 \rightarrow {}^7F_J$ (J = 0,1,2) transitions can produce sharp PL peaks in the range of 695–710 nm. These peaks are also found in the PL spectra of Sm-doped and codoped films under excitation with 407 nm laser line which corresponds to direct excitation of Sm^{3+} ions (Fig. 11c).

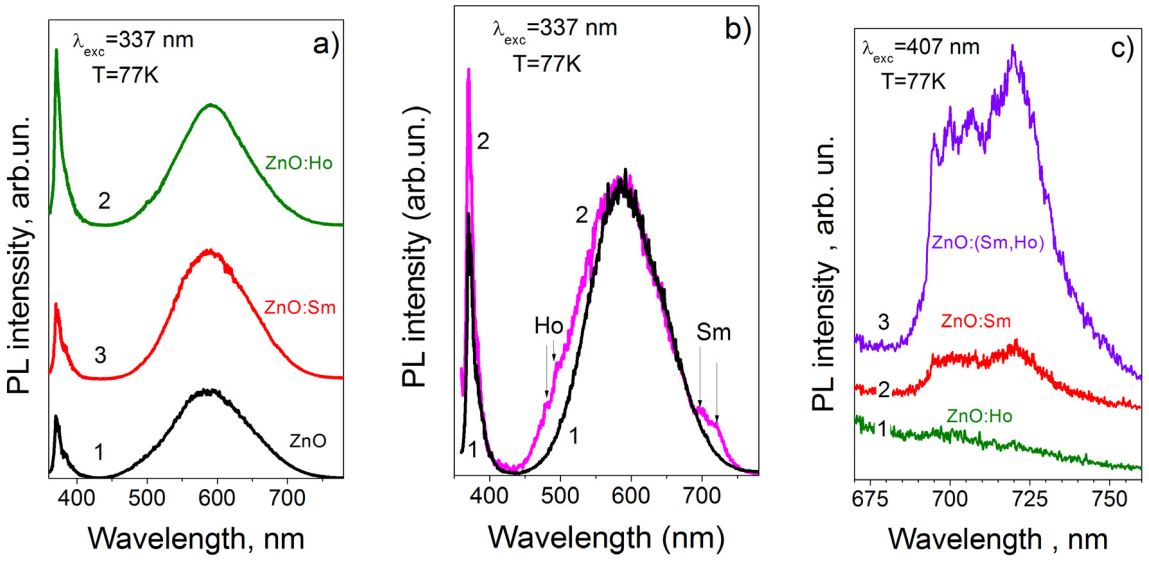

Figure 11. (a) PL spectra of undoped ZnO (1), ZnO: Ho (2) and ZnO: Sm (3) films; (b) normalized PL spectra of undoped (1) and (Sm, Ho) codoped (2) ZnO films; (c) PL spectra of ZnO: Ho (1), ZnO: Sm (2) and (Sm, Ho) codoped ZnO (3) films. Excitation wavelength λ_{EXC} = 337.1 nm (a, b) and 407 nm (c), T = 77 K.

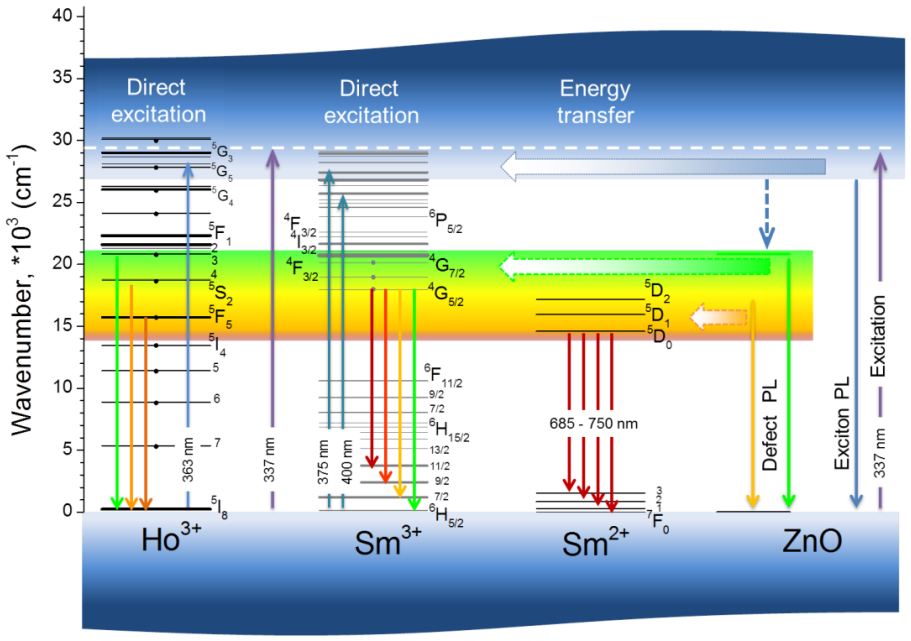

Figure 12. Schematic presentation of absorption and emisison transitions in Ho^{3+}, Sm^{3+}, Sm^{2+} ions in ZnO host.

The mechanism for Sm^{3+} to Sm^{2+} reduction is still debated. It has been supposed that it follows the reaction as $Sm^{3+} + e^{-} = Sm^{2+}$ and the stability of Sm^{2+} ions is determined by the oxygen-lack environment, i.e. by oxygen vacancies [33]. In such a case, when the Sm^{3+} ion inserted in host lattice captures a photogenerated electron, a metastable Sm^{2+} appears. Due to band bending at the grain surface, the photogenerated holes will migrate towards the surface and recombine with electrons trapped at the surface levels or convert metastable Sm^{2+} ions into stable Sm^{3+} ones [33].

It should be noted that PL intensity from RE ions is rather low and is observed al low temperatures only. At the same time, the PL spectrum excited with 337 nm laser line which cannot excite directly Ho^{3+} and Sm^{3+} ions also shows RE ion emissions of intensity comparable with those of native defects. This implies an energy transfer from ZnO lattice to RE ions, and the native ZnO defects can be considered as a pathway for this process (Fig.12).

3. Conclusion

In order to reveal the possibility of producing effective UV- and visible-light emitting phosphors using ZnO and ZnO-based compounds, the emission of undoped and doped ZnO, ZnMgO and ZnMgO–TiO_2 ceramics as well as ZnO polycrystalline screen-printed films was studied.

Defect-related emission of undoped ZnO ceramics exhibited itself in blue-orange spectral region and was shown to include green (515 nm), orange (610 nm) and red (720 nm) self-activated bands as well as the band related to residual Cu impurity (540 nm). The doping with Li and Ag led to the appearance of bright PL bands at 600 and 580 nm, respectively. Alloying ZnO with MgO was found to cause some blueshift of green self-activated as well as Li- and Ag-related bands, while Cu-related as well as orange and red self-activated ones did not change their positions, which indicated different interaction of corresponding emission centers with the host lattice. It was shown that the introduction of TiO_2 into the mixture of zinc and magnesium oxides resulted in the appearance of bright red PL band at 670 nm. The comparison of PL and PLE spectra for ZnMgO alloys and ZnMgO–TiO_2 composites led to the conclusion that the red band was due to the inclusions of Mg_2TiO_4 titanate formed in ZnMgO matrix under sintering. As a result, the emission of ZnMgO–TiO_2 composites consists of broad blue-orange and distinct red bands and is perceived by the naked eye as bright white light.

The screen-printed undoped ZnO films showed intense UV and weak defect-related emissions when being sintered at temperatures lower than 800 °C. At higher temperatures, the UV luminescence decreased and the self-activated defect-related PL increased. The doping of ZnO films with Li at 800 °C enabled to enhance UV emission and to improve structural properties of the films. It is found that the effect of Li-doping on the PL properties of ZnO films is closely connected with the influence of Li on the development of film microstructure via the control of crystal sizes and concentration of native point defects. In the PL spectra of Ho and Sm codoped ZnO, the PL peaks ascribed to optical transitions in Ho^{3+} and Sm^{2+} ions were identified, and the mechanism of Sm^{3+} to Sm^{2+} reduction was discussed.

Obtained results show that intense UV emission can be obtained in polycrystalline screen-printed ZnO films by corresponding heat treatment. At the same time, ZnMgO–TiO_2 composites can be considered as promising materials for white-light emitters.

Acknowledgments

This work was supported by the National Academy of Science of Ukraine via the projects III-10-12 and III-10-15. We also would like to thank Yu.O. Polishchuk for XRD measurements.

Conflict of Interest

The authors declare no conflicts of interest regarding this paper.

References

1. Ozgür U, Alivov YI, Liu C, et al. (2005) A comprehensive review of ZnO materials and devices. *J Appl Phys* 98: 041301 (1–102).
2. Kuz'mina IP, Nikitenko VA (1984) *Zinc oxide. Production and optical properties*, Moscow: Nauka, 1–166, in Russian.
3. Fan JC, Chang SL, Xie Z (2013) *ZnO-based light-emitting diodes (Ch. 2)* in Optoelectronic—Advanced Materials and Devices, Pyshkin S and Ballato J M (Eds.), ISBN: 978-953-51-0922-8, InTech, DOI: 10.5772/51181.
4. Markevich I, Stara T, Kolomys O, et al. (2014) Influence of annealing in Zn vapor on the luminescence of MgZnO ceramics. *Phys Stat Sol C* 11: 1485–1487.
5. Markevich IV, Stara TR, Bondarenko VO (2015) About self-activated orange emission in ZnO. *Semicond Phys Quantum Electron Optoelectron* 18: 134–137.
6. Markevich IV, Stara TR, Bondarenko VO (2015) Influence of Mg content on defect-related luminescence of undoped and doped MgZnO ceramics. *Semicond Phys Quantum Electron Optoelectron* 18: 344–348.
7. Borkovska LV, Stara TR, Markevich IV (2016) Photoluminescence in composite ceramics prepared of zinc, magnesium and titanium oxides. The 2016 E-MRS Spring Meeting, Symposium N, abs. N.13.23, Lille, France.
8. Khomenkova L, Kushnirenko VI, Osipyonok MM, et al. (2015) Structural, electrical and luminescent properties of ZnO:Li films fabricated by screen-printing method on sapphire substrate. *Phys Stat Sol C* 12: 1144–1147.
9. Khomenkova L, Kushnirenko VI, Osipyonok MM, et al. (2015) Effect of rare-earth doping on structural and luminescent properties of screen-printed ZnO films. *ECS Trans* 66: 321–332.
10. Osipyonok M, Pekar G, Syngaivskyy O (2011) The method of fabrication of solid layers by screen printed approach. Patent of Ukraine 94561 (10.05.2011).
11. Studenikin SA, Golego N, Cocivera M (1998) Fabrication of green and orange photoluminescent undoped ZnO films using spray pyrolysis. *J Appl Phys* 84: 2287–2294.
12. Lauer RB (1973) The IR photoluminescence emission band in ZnO. *J Phys Chem Sol* 34: 249–253.
13. Ong HC, Du GT (2004) The evolution of defect emissions in oxygen-deficient and -surplus ZnO thin films: the implication of different growth modes. *J Cryst Growth* 265: 471–473.
14. Kang HS, Kim JW, Lim SH, et al. (2006) Investigation on the variation of green, yellow and orange emission properties of ZnO thin films. *Superlattices Microstruct* 39: 193–201.

15. Nikitenko VA, Tarkpea KÉ, Tereshchenko AI, et al. (1989) Red luminescence in zinc oxide. *J Appl Spectroscopy* 51: 986–989.
16. Gerbstein YM, Zelikin YM (1969) About the origin of the centers of yellow-orange luminescence in zinc oxide (in Russian). *Optika i Spectroskopiya* 27: 515–518.
17. Ohtomo A, Kawasaki M, Koida T, et al. (1998) $Mg_xZn_{1-x}O$ as a II–VI widegap semiconductor alloy. *Appl Phys Lett* 72: 2466–2468.
18. Markevich IV, Stara TR, Kuchuk AV, et al. (2014) Formation of MgZnO alloy under thermodynamic conditions. *Physica B* 453: 153–156.
19. Kushnirenko VI, Markevich IV, Zashivailo TV (2012) Acceptors related to group I elements in ZnO ceramics. *J Lumin* 132: 1953–1956.
20. Dittmann R, Hahn D (1967) Zum lumineszenzmodell manganaktivierter titanate. *Z Phys* 207: 484–499.
21. Qui Z, Luo T, Zhang J, et al. (2015) Effectively enhancing blue excitation of red phosphor $Mg_2TiO_4:Mn^{4+}$ by Bi^{3+} sentisization. *J Lumin* 158: 130–135.
22. Song CF, Qui T, Yuan HF, et al. (2010) Enhanced green emission in ZnO/zinc titanate composite materials. *Mater Sci Eng B* 175: 243–247.
23. Akilan T, Srinivasan N, Saravanan R (2015) Magnetic and optical properties of Ti doped ZnO prepared by solid state reaction method. *Mater Sci Semicond Proc* 30: 381–387.
24. Wardle MG, Goss JP, Briddon PR (2005) Theory of Li in ZnO: a limitation for Li-based p-type doping. *Phys Rev B* 71: 155205.
25. Zhang Z, Knutsen KE, Merz T, et al. (2012) Thermal process dependence of Li configuration and electrical properties of Li-doped ZnO. *Appl Phys Lett* 100: 042107.
26. Meyer BK, Stehr J, Hofstaetter A, et al. (2007) On the role of group I elements in ZnO. *Appl Phys A* 88: 119–123.
27. Ohashi N, Ebisawa N, Sekiguchi T, et al. (2005) Yellowish-white luminescence in codoped zinc oxide. *Appl Phys Lett* 86: 091902.
28. Rauch C, Gehlhoff W, Wagner MR, et al. (2010) Lithium related deep and shallow acceptors in Li-doped ZnO nanocrystals. *J Appl Phys* 107: 024311.
29. Chand P, Gaura A, Kumar A, et al. (2014) Structural, morphological and optical study of Li doped ZnO thin films on Si (100) substrate deposited by pulsed laser deposition. *Ceramics Int* 40: 11915–11923.
30. Farid S, Mukherjee S, Sarkar K, et al. (2016) Enhanced optical properties due to indium incorporation in zinc oxide nanowires. *Appl Phys Lett* 108: 021106.
31. Blasse G, Grabmaier BC (1994) *Luminescent Materials*, Berlin–Heidelberg: Springer–Verlag, 233.
32. Hsu CL, Chang SJ (2014) Doped ZnO 1D nanostructures: synthesis, properties, and photodetector application. *Small* 10: 4562–4585.
33. Bachir S, Azuma K, Kossanyi J, et al. (1997) Photoluminescence of polycrystalline zinc oxide co-activated with trivalent rare earth ions and lithium. Insertion of rare-earth ions into zinc oxide. *J Lumin* 75: 35–49.